Time cells in the human hippocampus and entorhinal cortex support episodic memory

Gray Umbach[a], Pranish Kantak[a], Joshua Jacobs[b], Michael Kahana[c], Brad E. Pfeiffer[d], Michael Sperling[e], and Bradley Lega[a,1]

[a]Department of Neurological Surgery, University of Texas Southwestern, Dallas, TX 75390; [b]Department of Biomedical Engineering, Columbia University, New York, NY 10027; [c]Department of Psychology, University of Pennsylvania, Philadelphia, PA 19104; [d]Department of Neuroscience, University of Texas Southwestern, Dallas, TX 75390; and [e]Department of Neurology, Thomas Jefferson University, Philadelphia, PA 19144

Edited by György Buzsáki, New York University Langone Medical Center, New York, NY, and approved September 23, 2020 (received for review June 30, 2020)

The organization of temporal information is critical for the encoding and retrieval of episodic memories. In the rodent hippocampus and entorhinal cortex, evidence accumulated over the last decade suggests that populations of "time cells" in the hippocampus encode temporal information. We identify time cells in humans using intracranial microelectrode recordings obtained from 27 human epilepsy patients who performed an episodic memory task. We show that time cell activity predicts the temporal organization of retrieved memory items. We also uncover evidence of ramping cell activity in humans, which represents a complementary type of temporal information. These findings establish a cellular mechanism for the representation of temporal information in the human brain needed to form episodic memories.

time cells | human electrophysiology | medial temporal lobe | theta precession

Episodic memory describes our ability to weave temporally contiguous elements into rich and coherent experiences. The formation of these memories requires the brain to represent temporal information, and recent discoveries in animal models of episodic memory suggest that the activity of "time cells" in the mesial temporal lobe (MTL) fulfills this critical role in memory formation (1–6). Like place cells, which exhibit an increased probability of firing at specific locations, or "place fields," within an environment, time cells reliably fire at specific and consistent moments, or "time fields," within a longer time interval (1, 2, 6). Previous work has demonstrated the specificity of these time cell sequences to task context (1, 4), a link between sequential firing patterns in the hippocampus and successful sequence memory (7), and unique mapping of specific time cell sequences to specific memory items (4). A clear implication of these findings is that time cells offer a specific mechanism for the representation of temporal contextual information in human episodic memory. Like place cells, time cells exhibit theta-phase precession (1), theoretically facilitating formation of item–context associations through spike timing-dependent plasticity (8–10). With these properties shared with place cells, time cells offer the potential of a unifying physiological mechanism for the representation of both spatial and temporal contexts in the hippocampus.

Complementing the identification of time cells, subsequent experiments in rodents identified a distinct population of temporally sensitive cells in the lateral entorhinal cortex (LEC) whose activity gradually rises or decays across a given time interval (termed "ramping cells") (11). As these cells are sensitive to contextual changes during experience, they could represent the slowly evolving nature of contextual information. Ramping cells may provide temporal information at slightly different scales than hippocampal time cells and may even modulate their activity (11–14), analogous to hexadirectional grid cells in spatial navigation (15–17). Together, time cells and ramping cells provide a mechanism for the representation of temporal information over timescales of seconds to minutes.

The characterization of time cells in rodents stimulated widespread interest among memory theorists, reflected in proposed models of episodic memory in which time cells play a critical role (12–14, 18, 19). To date, however, time cells have not been reported in humans, and it is unknown if they support episodic memory. We addressed this critical gap in knowledge using a unique dataset of 27 human surgical epilepsy patients implanted with microelectrodes in the hippocampus and entorhinal cortex. We identified populations of single neurons during memory encoding and retrieval in which temporal location within behavioral epochs consistently modulated spiking activity, controlling for the effects of recall success and other covariates. We found that these time cells exhibit theta-phase precession during memory encoding, and we identify a population of ramping cells more prevalent in the entorhinal cortex. We then identify key behavioral properties of these human time cells, demonstrating that their activity correlates with the tendency of subjects to use temporal information to link memory items together at the time of retrieval. We place these findings within the context of existing experimental and theoretical treatments of human episodic memory.

Results

Behavioral Task and Unit Isolation. To investigate whether time cells exist in humans and characterize their potential relationship to episodic memory, we used microelectrode recordings (*SI Appendix*, Fig. S1) obtained in 27 human participants (*SI Appendix*, Table S1) who performed the free recall task (Fig. 1*A*), a standard assay of episodic memory. The structure of the task,

Significance

Time cells are neurons in the hippocampus and entorhinal cortex that fire at specific moments within a cognitive task or experience. While many prominent theories of memory encoding offer time cells as the source of the temporal component to memory, they have never been observed in human recordings. We identify time cell populations in the medial temporal lobe of humans during memory encoding and retrieval. Further, we demonstrate that the stability of the time signal provided by time cells during encoding influences the ability to temporally order memories at time of retrieval.

Author contributions: G.U., J.J., M.K., B.E.P., and B.L. designed the research; G.U., P.K., M.S., and B.L. performed the research; G.U. analyzed the data; J.J., M.K., and B.E.P. reviewed and edited the manuscript; B.L. supervised the project; and G.U. and B.L. wrote the paper.

The authors declare no competing interest.

This article is a PNAS Direct Submission.

[1]To whom correspondence may be addressed. Email: Bradley.Lega@UTSouthwestern.edu.

This article contains supporting information online at https://www.pnas.org/lookup/suppl/doi:10.1073/pnas.2013250117/-/DCSupplemental.

First published October 27, 2020.

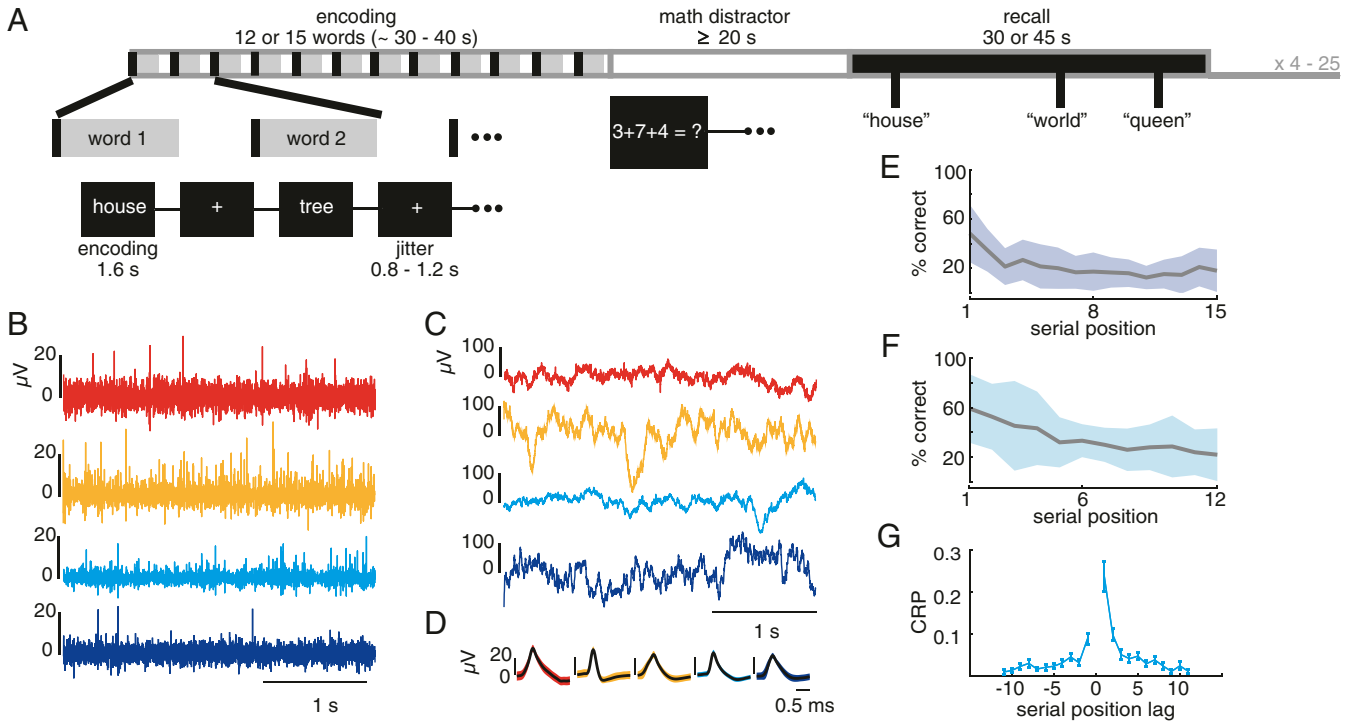

Fig. 1. Task and performance. (*A*) Free recall task. (*B*) Noise-subtracted and band-passed (300- to 1,000-Hz) signal from four different channels used for single-unit isolation. (*C*) Noise-subtracted and low-passed (<300-Hz) signal. (*D*) Mean waveforms of time cells extracted from the channels displayed in *B*. (*E*) Recall performance by encoding list serial position for all recording sessions with 15-word lists ($n = 18$). (*F*) The same as *D* but for all recording sessions with 12-word lists ($n = 6$). Shaded regions represent ±1 SD. (*G*) Conditional response probability (CRP) vs. serial position lag demonstrating the increased likelihood of consecutively recalling items encoded at temporally adjacent serial positions.

with consistent and well-defined time segments for each item encoding list and each retrieval period, facilitated our ability to detect time cells. In the task, participants studied lists of common nouns presented regularly over the course of a 1.6-s encoding interval. Following an arithmetic distractor task, participants freely recalled as many words as they could remember. For sessions with 12-word encoding lists, the encoding period lasted roughly 30 s, and participants had 30 s for retrieval. For sessions with 15-word lists, the encoding period lasted roughly 40 s, and participants had 45 s for retrieval. They completed an average of 15.3 item lists, successfully remembering an average of 24.2 ± 11.6% of the memory items. Behavioral performance during these sessions exhibited expected patterns (20), including greater recall accuracy for the initial list items and evidence of temporal contiguity in recall patterns (Fig. 1 *E*–*G*).

We isolated a total of 768 single units from the implanted microelectrodes (Fig. 1 *B*–*D*), calculating standard quality metrics that were comparable with previously published data describing human MTL neurons (*SI Appendix*, Fig. S2 and Table S2) (21). We only considered neurons with confirmed localizations within the MTL ($n = 734$) (*Materials and Methods*). In accordance with previous studies identifying time cells in the rodent hippocampus and medial entorhinal cortex (MEC), we focused our analysis on the 509 putative pyramidal neurons isolated from the hippocampus and entorhinal cortex ($n = 458$ and 51, respectively, from each region, defined by spike width and firing rate) (*Materials and Methods*) (1–3, 5, 22).

Single Neurons in the Human Hippocampus and Entorhinal Cortex Encode the Passage of Time. To represent temporal information, time cells fire at a preferred time interval—their time field—that is defined relative to the beginning and end of a period of fixed duration. Both the encoding and retrieval periods of the free recall task were of relatively fixed duration, facilitating time cell identification. We used normalized time, with zero representing the beginning of the encoding or retrieval list and one representing its end, for time cell analyses to account for slight differences in encoding list length secondary to random interstimulus jitter (*Materials and Methods*). To identify time cells, we looked for an interaction between time and firing rate using a nonparametric ANOVA across time bins (Kruskal–Wallis test) after generating session-wide firing rate tuning curves with Gaussian convolution of the spike trains (*Materials and Methods*). Significance testing incorporated a permutation procedure, in which we repeated the ANOVA 1,000 times after circularly shuffling the original tuning curve (*Materials and Methods*). We identified significant populations of time cells during encoding (79/509 total pyramidal neurons, $P < 0.001$, binomial test) as well as retrieval (60/509 neurons, $P < 0.001$, binomial test). Example time cells, exhibiting characteristic firing within a preferred temporal window, are shown in Fig. 2 (encoding) and Fig. 3 (retrieval). We additionally confirmed that the number of time cells observed across participants was greater than the number identified following shuffling the spike trains for both encoding [$t(25) = 4.44$, $P < 0.001$] and retrieval [$t(25) = 4.01$, $P < 0.001$]. We observed time cells in 25 of 26 subjects in whom we isolated at least one pyramidal cell.

We conducted several control analyses to ensure that identification of temporally modulated spiking activity was not dependent upon parameters such as the number of time bins used in the nonparametric test or the SD of the Gaussian kernel, our specific binning procedure, the influence of covariates such as item onset and recall success (*SI Appendix*, Fig. S3 *A* and *B*), or the specific time cell identification framework more generally (6, 23) (*SI Appendix*, Fig. S3 *C*–*F* and Tables S3 and S4). Encoding

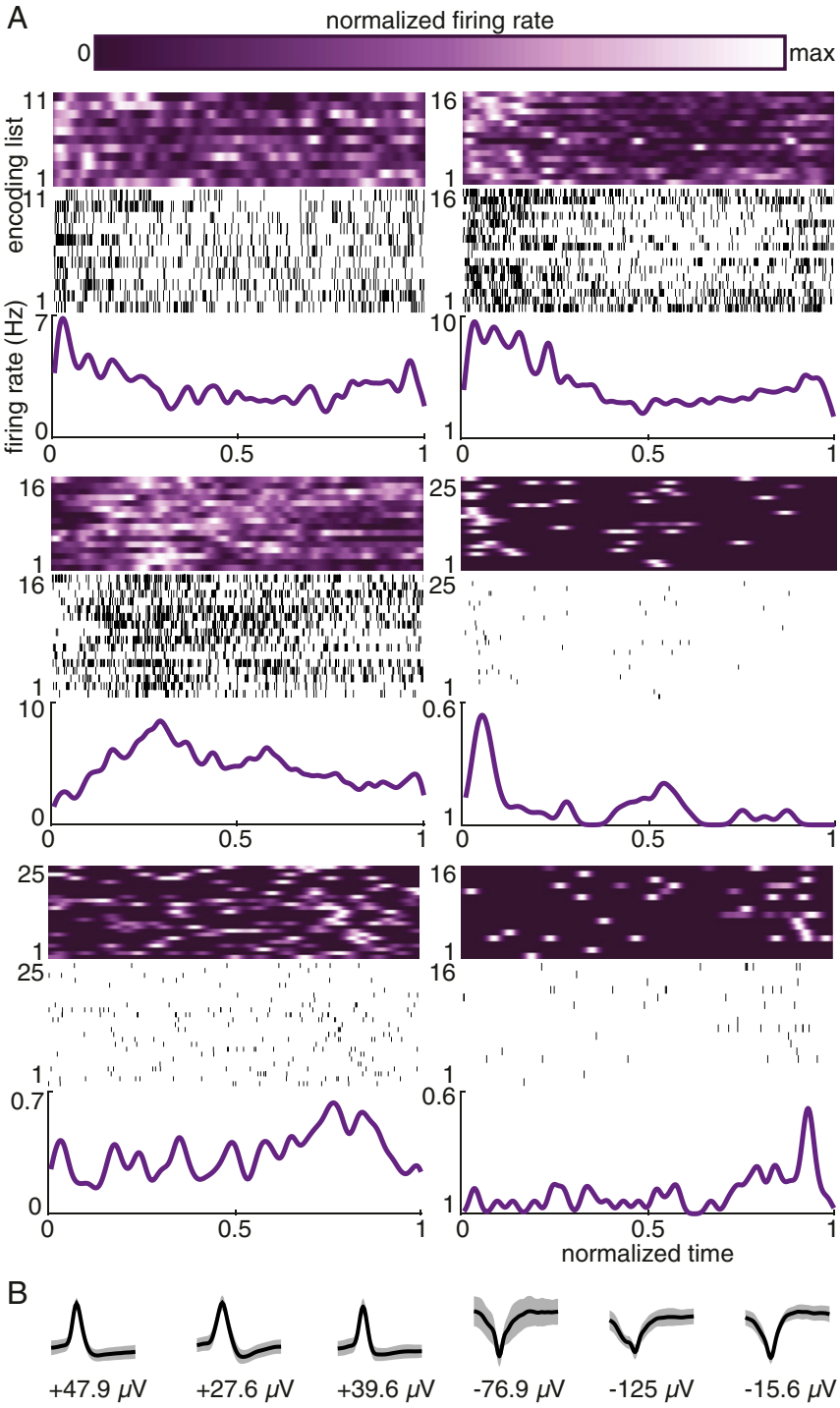

Fig. 2. Time cells activate at specific moments during memory encoding. (*A*) Six examples of encoding time cells. Spike heat map (*Top*), spike raster (*Middle*), and PSTH (*Bottom*) plotted against normalized encoding list time. (*B*) Mean spike waveforms and peak voltages of cells whose data are display in *A*. From left to right, waveforms in *B* correspond to cells in *A* from *Top Left* to *Bottom Right*. The *x* axis represents normalized time, with zero marking the beginning of the encoding list and one the end. Encoding lists lasted from 30 to 40 s and were nearly equivalent across lists for each subject.

success did not predict time cell firing [$z(71) = 0.071$, $P > 0.2$, rank sum test] (*SI Appendix*, Fig. S4).

For each time cell, we identified time fields as epochs of elevated firing rate across encoding lists or retrieval periods (*Materials and Methods*). A key property of time cells is that, in aggregate, they should represent time throughout a given epoch, analogous to place cells. Across all participants, this is what we observed when plotting the peristimulus time histograms (PSTHs) after ordering each cell by its preferred time field (Fig. 4 *A*–*D*). Similar to previous reports of time cells in rodents, we observed denser temporal representation at early and late epochs (6, 23, 24). Of the 79 total encoding time cells and 60 total retrieval time cells, 16 behaved as time cells in both periods, supporting previous work demonstrating context-dependent recruitment of unique subsets of time cells that partially overlap (1, 4, 23) (Fig. 4*E*). However, we found no evidence of correlation between the time

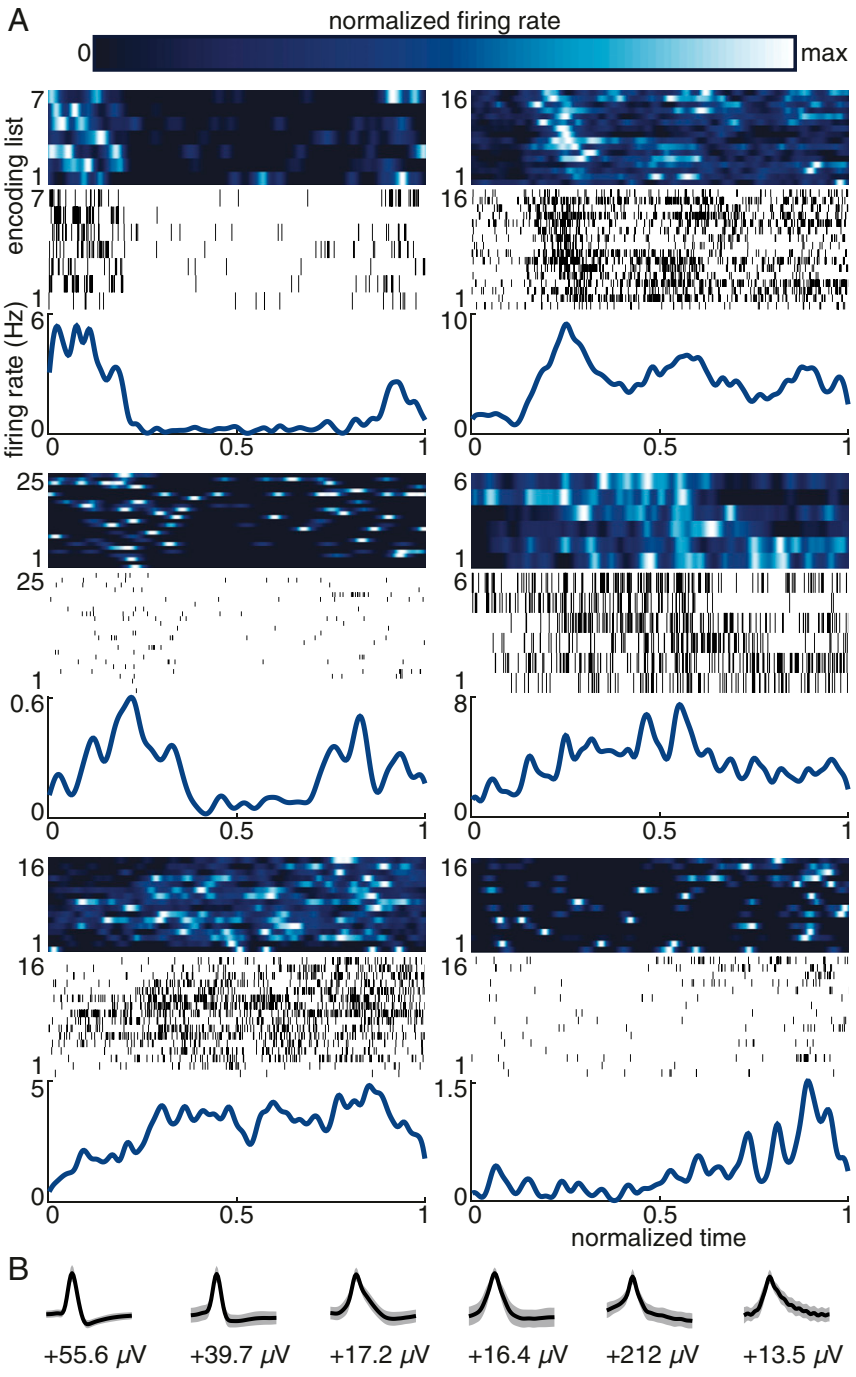

Fig. 3. Time cells activate at specific moments during memory retrieval. (*A*) Six examples of retrieval time cells. Spike heat map (*Top*), spike raster (*Middle*), and PSTH (*Bottom*) plotted against normalized retrieval period time. (*B*) Mean spike waveforms and peak voltages of cells whose data are display in *A*. From left to right, waveforms in *B* correspond to cells in *A* from *Top Left* to *Bottom Right*. The *x* axis represents normalized time, with zero marking the beginning of the retrieval period and one the end. Retrieval periods lasted either 30 or 45 s but were consistent for each subject.

of peak firing during encoding and retrieval in these cells ($r = 0.19$, $P > 0.2$, Spearman rank correlation) (Fig. 4*F*). The identification of time cells during retrieval in free recall, when participants recall items without any cue information, makes it unlikely that our methods identify cells responding to item stimuli generally.

Temporal Representation Is Not Significantly Different along the Anterior–Posterior Hippocampal Axis. A unique feature of our dataset compared with previous human microelectrode experiments was the availability of recordings from both the anterior and posterior hippocampus. Of the 79 encoding time cells, we isolated 34 time cells from the anterior hippocampus and 22 from the posterior hippocampus. We isolated 30 and 19 retrieval time cells from the anterior and posterior hippocampus, respectively. These recordings provided an opportunity to compare the width of time fields for anterior vs. posterior hippocampal time cells, motivated by the well-known finding that rodent place cells exhibit wider fields in the ventral (analogous to anterior) compared with dorsal (analogous to posterior) hippocampus (25, 26). However, we observed no significant difference in time field duration according to

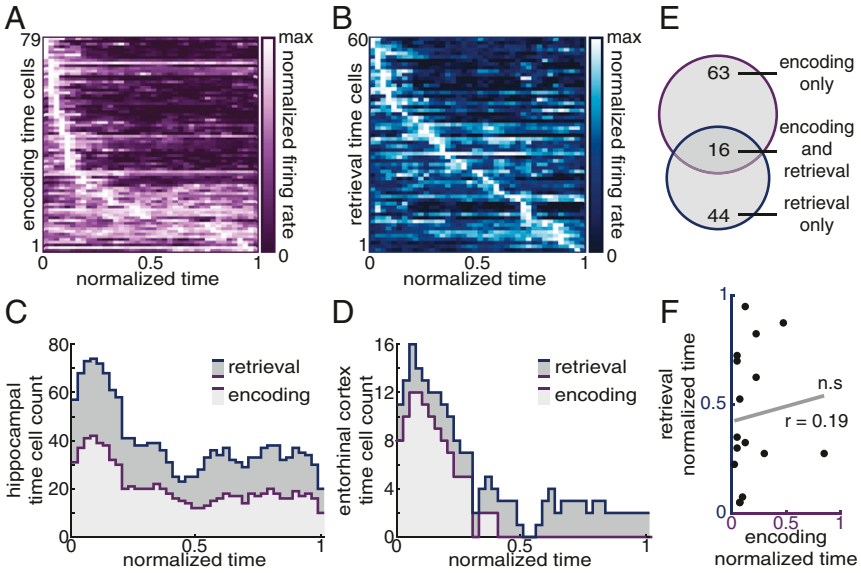

Fig. 4. Overlapping but distinct encoding and retrieval time cell ensembles. (*A*) Encoding time cell firing rate heat map with rows organized by the time of the peak in the PSTH. (*B*) Retrieval time cell firing rate heat map with rows organized by the time of the peak in the PSTH. (*C*) Count of hippocampal encoding and retrieval time cells with a time field covering each time bin. (*D*) Count of entorhinal encoding and retrieval time cells with a time field covering each time bin. (*E*) Overlap between encoding and retrieval time cell populations. (*F*) Correlation between the peak firing rate time bin during the encoding period and the peak firing rate time bin during the retrieval period for time cells active during both memory behavior epochs. n.s., not significant.

longitudinal location along the hippocampus for either encoding [median duration 2.52 vs. 2.59 s, respectively; $z(131) = 0.16$, $P > 0.2$, rank sum test] or retrieval [median duration 3.38 vs. 3.26 s, respectively; $z(136) = -0.72$, $P > 0.2$, rank sum test] time cells (*SI Appendix*, Fig. S5). Time field onset time also did not differ between anterior and posterior time cells [encoding: $z(52) = -1.06$, $P > 0.2$; retrieval: $z(46) = -0.11$, $P > 0.2$, rank sum test] (*SI Appendix*, Fig. S5).

Further, we did not observe significant differences in time cell behavior based on hippocampal vs. entorhinal recording location. Of the 123 total time cells, we localized 103 to the hippocampus and 20 to the entorhinal cortex. The ensemble activity of both populations represented time across the duration of the behavioral period (Fig. 4 *C* and *D*). Location did not significantly affect either the duration of the time field [$z(349) = -1.06$, $P > 0.2$] (*SI Appendix*, Fig. S3*G*) or the onset of the time fields [$z(129) = 1.08$, $P > 0.2$] (*SI Appendix*, Fig. S3*H*).

The Entorhinal Cortex Is Enriched in Neurons That Demonstrate Ramping Activity across Multiple Timescales. We asked whether ramping cells can also be found in the human MTL. These cells exhibit spiking activity that increases or decreases across the duration of a temporal epoch (11, 27, 28). Following the methodology established by Tsao et al. (11), we built a generalized linear model for each cell (*Materials and Methods*). We included 10 predictor variables in the model (*SI Appendix*, Fig. S6). Two were related to time: session time, which continuously tracked absolute elapsed time since the first second of the experimental recording session (longer context duration), and epoch time, which tracked the absolute elapsed time within a given behavioral epoch such as a single encoding list (shorter context duration). We additionally included covariates such as word onset, recall success, list onset, and vocalization, along with a categorical predictor variable indicating whether the subject was in the encoding or retrieval period of the task (*SI Appendix*).

Relative to the hippocampus, we found entorhinal cortex neurons more frequently responded to the temporal predictors of the model (Fig. 5 and *SI Appendix*, Fig. S6*B*). The difference in ramping cell proportion between MTL regions was significant for all ramping cells collectively [25/51 in the entorhinal cortex vs. 158/458 in the hippocampus, $\chi^2(1) = 4.2$, $P = 0.040$] as well as for those that specifically tracked session time [21/51 vs. 124/458, $\chi^2(1) = 4.5$, $P = 0.034$] and epoch time [13/51 vs. 56/458, $\chi^2(1) = 6.9$, $P = 0.0087$]. However, the regions did not significantly differ for any other predictor (Fig. 5*B*). This finding is consistent with the known properties of ramping cells in rodents, where this phenomenon is localized to the LEC (11). Ramping MTL neurons exhibited a wide range of time constants (*SI Appendix*, Fig. S6*D*) and displayed both "up" ramping and "down" ramping (Fig. 5*A*). Of the 145 cells demonstrating ramping across the session (longer timescale), 67 exhibited up ramping, and 78 exhibited down ramping. Of the 69 cells demonstrating ramping within behavioral epochs (the encoding or retrieval period of a single item list), 18 exhibited up ramping, and 51 exhibited down ramping. Results of a control analysis in which ramping cells were identified after splitting the data are shown in *SI Appendix*, Table S5.

Time Cells Exhibit Theta-Phase Precession during Item Encoding. Given previous findings (1), we hypothesized that time cells may exhibit phase precession, although this properly has not been demonstrated in human place cells (or time cells) to date. We employed an established circular–linear method for measuring phase precession (29), a method well-suited to analyze precession with lower spike counts (29, 30). We focused on the firing of time cells within their preferred time fields. For time cells with multiple time fields, we defined the preferred time field as the one with the highest peak firing rate. We measured the theta-phase angle for all spike events in a time cell's preferred time field. We evaluated precession within the 2- to 10-Hz range, encompassing frequencies that exhibit mnemonically relevant properties in humans such as phase locking, phase reset, and power increases during successful memory encoding (31–33).

Twenty-four encoding time cells demonstrated significant phase precession, which we identified by measuring a significant correlation between time and phase at one or more of these frequencies ($P = 0.0067$, binomial test, corrected for multiple comparisons with $Q = 0.2$) (Fig. 6 *A* and *C*). These counts

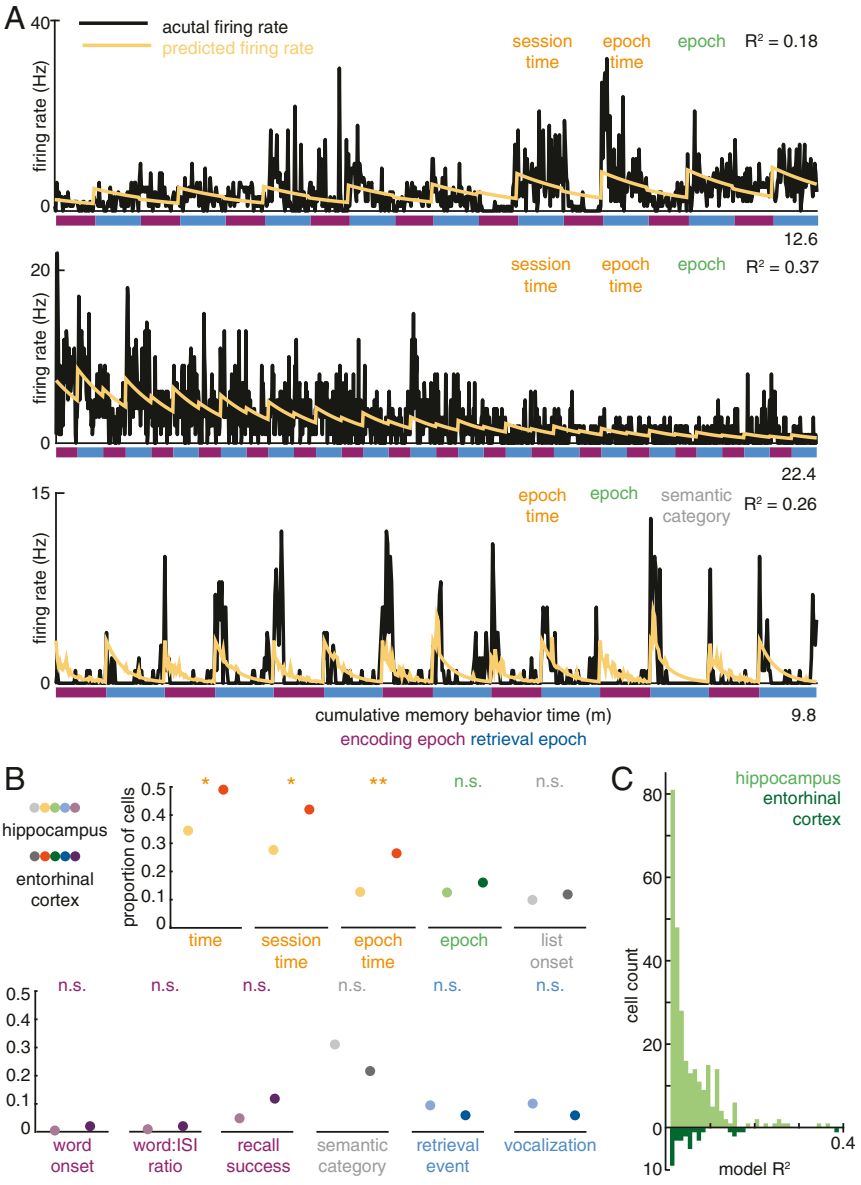

Fig. 5. The entorhinal cortex is enriched in cells that track time at multiple timescales simultaneously. (*A*) Three examples of ramping cells. The actual and model-predicted firing rates for each cell are superimposed. Data are from encoding (purple bars under axes) and retrieval periods (blue bars under axes). The model R^2 and added predictors are displayed to the top right of each cell's firing rate curve. (*B*) Comparison of the fraction of hippocampal and entorhinal cells' firing rate predicted by each variable. (*C*) Histogram of the model R^2 values for hippocampal (light green) and entorhinal (dark green) populations. n.s., not significant. $*P < 0.05$; $**P < 0.01$.

significantly exceeded that expected based on shuffle controls (time and phase shuffling, $P = 0.001$ and 0.004, respectively). We tested for significant phase precession across the entire population of encoding time cells by comparing the distribution of correlation coefficients from circular–linear regression against a shuffle distribution, revealing significant precession overall ($P = 0.026$) (*SI Appendix*, Fig. S7*C*). Similar to theta precession described in rodents for place cells (34), peak firing within the time field occurred near the trough of the theta cycle (95% CI for phase in the central 25% of the time field: 110° to 197°, $z = 4.03$, $P = 0.017$, Rayleigh test) (Fig. 6*B*). These encoding time cells had a mean precession rate of −69 ± 45°/s and median correlation coefficient of −0.30 between phase and time. Consistent with expectations from rodent findings (10), we detected significant theta local field potential (LFP) power increases during the time fields of precessing cells relative to behavioral periods outside of their time fields [$t(41) = 2.86$, $P = 0.0067$].

In a convergent analytical approach, we also tested for significant precession across all encoding time cells using a separate published method (35). We observed an association between the firing rate of all encoding time cells and the phases of their spikes ($r = -0.59$, $P = 0.040$, one-sided Spearman rank correlation, $P = 0.0093$, nonparametric circular ANOVA) (Fig. 6*D*). We found that as cell firing rate increased, spike phase precessed to earlier phases of the theta cycle. Further, as in rodents (35), as encoding time cell firing rate began to decelerate from local maxima, phase precession continued ($r = 0.89$, $P < 0.001$, one-sided Spearman rank correlation) (Fig. 6*F*). Consequently, as time cells entered time periods of sustained elevations in firing rate (such as the beginning of their time field), they fired at consistently later theta phases than when exiting periods of

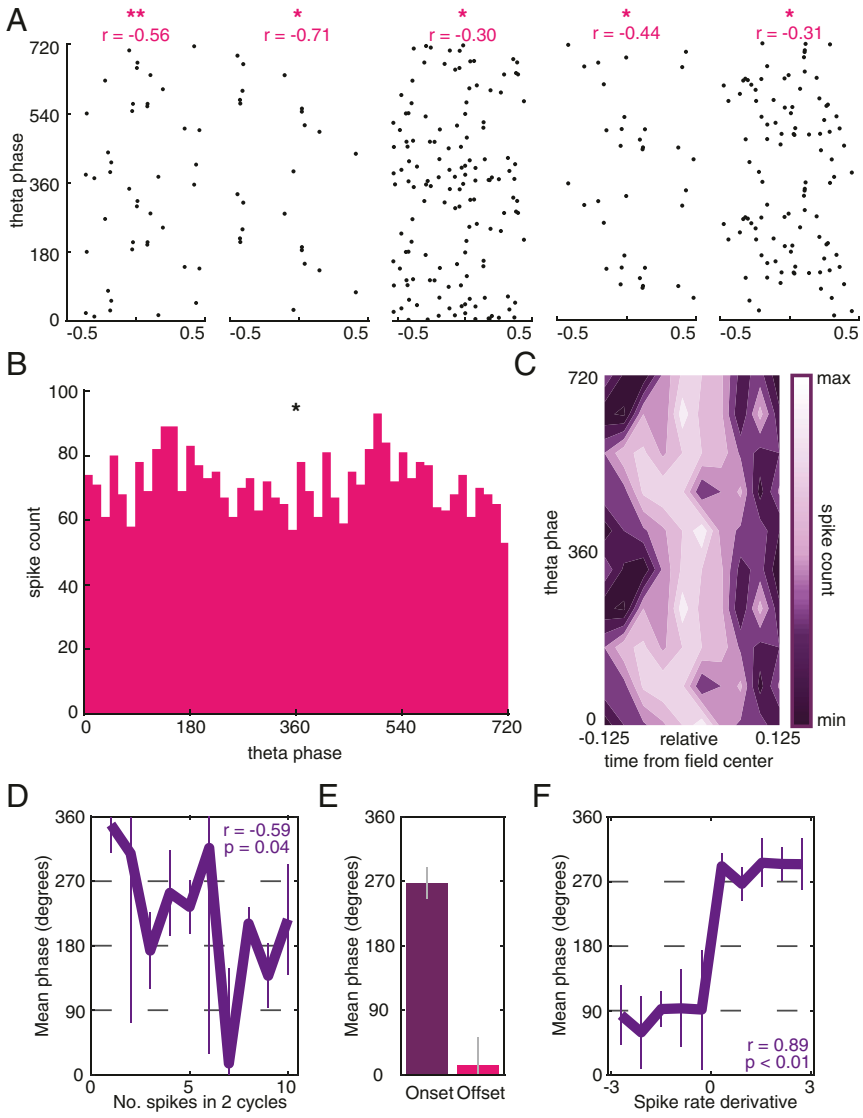

Fig. 6. Time cells demonstrate theta-phase precession during memory encoding. (*A*) Example phase–time plots for five example encoding time cells in their preferred time field. The circular–linear correlation coefficient value is shown above (29). (*B*) Phase histogram of spikes falling within the central 25% of the time fields of all encoding time cells demonstrating precession. (*C*) Heat map of spike counts obtained by superimposing the central 25% (centered on the time of peak time cell activity) of the phase–time plots from all encoding time cells demonstrating significant precession. (*D*) Correlation between encoding time cell firing rate and spike phase (22). Error bars represent the 95% CI. (*E*) Circular mean phase at onset of spike acceleration (dark purple) compared with circular mean phase at offset of spike deceleration (*Materials and Methods*). (*F*) Correlation between spike rate derivative (acceleration) and spike phase. Error bars represent the 95% CI. $*P < 0.05$; $**P < 0.01$.

sustained firing rate increases (such as the termination of their time field; $P = 0.0068$, nonparametric circular ANOVA) (Fig. 6*E*).

We did not observe significant time cell population-level precession during retrieval based on either circular–linear correlation coefficients ($P = 0.070$) or rate and rate derivative correlations with spike phase (*SI Appendix*, Fig. S7). We examine the overall magnitude of precession in human time cells as well as possible implications of the encoding/retrieval dissociation related to the mnemonic relevance of the immediate temporal context during which time cells are observed in *Discussion*.

Stability in Time Cell Firing Patterns Promotes Temporal Clustering of Memory Items. We analyzed the relationship between time cell activity and memory behavior, asking whether firing patterns of time cells are associated with the tendency of human subjects to remember items presented adjacent to one another in time during encoding (quantified using the temporal clustering factor [TCF]) (36, 37). The TCF communicates the degree to which subjects group memory items at retrieval based on their temporal proximity at encoding, with a value of zero representing no preservation of order between encoding and retrieval and a value of one representing perfect recapitulation (*Materials and Methods*). We considered the possibility that the temporal clustering of memory items relies directly on the temporal contextual information that is provided by time cells. In rodents, variation of time cell firing relative to a preferred time field predicts future memory errors (1), and we therefore hypothesized that this same type of variability would predict decreased temporal clustering. We reasoned that less precision in the signal provided by time cells would decrease participants' ability to temporally cluster items. We used an estimate of time cell firing consistency calculated as

the average similarity between a time cell's firing pattern on a single item list and its average firing pattern across all lists. We termed this parameter ρ (Fig. 7 *A* and *B* and *Materials and Methods*). Higher ρ means that a cell's firing pattern remains consistent across encoding lists, while lower ρ indicates greater variability in firing patterns across lists. Partitioning time cells into those with high and low ρ values (split at the median), we found that those with higher ρ are associated with greater temporal clustering of items by subjects at the time of memory retrieval [$z(77) = 2.56$, $P = 0.011$, rank sum test] (Fig. 7*C*). This finding supports a link between the fidelity of temporal information provided by time cells and the tendency of participants to use temporal information when retrieving memory items.

We did not find an association between ρ and semantic clustering [$z(77) = -1.21$, $P > 0.2$], indicating that consistency of time cell firing specifically predicts the temporal organization of memories and not clustered memories more generally. Further, consistent temporal representation provided by time cells (higher ρ values) increased the likelihood that individuals would recall memory items located within a time cell's preferred field (Fig. 7*D*) [$z(70) = 2.23$, $P = 0.025$, rank sum test], although ρ did not significantly predict overall performance (Fig. 7*E*) [$z(77) = -1.93$, $P = 0.054$, rank sum test]. This latter result likely reflects the fact that several variables beyond temporal contextual information affect performance in the free recall task. Additional behavioral analyses for time cells, especially related to the encoding of primacy items, are shown in *SI Appendix*, Fig. S8.

Discussion

The Implications of Human Time Cells. The ability to represent time is fundamental to episodic memory, in which item information ("what") is linked precisely to temporal information ("when") to create the complex and coherent experiences of "mental time travel" central to human experience (38). The existence of time cells in rodents with properties analogous to place cells sparked significant interest among both human and rodent memory researchers because time cells offer a unifying mechanism for the representation of both spatial and temporal context. The demonstration of time cells in humans lends critical support to prominent models of memory positing that temporal coding mechanisms are central to the process of associative memory (36, 39). In contrast to the direct representation of temporal context provided by these cells, previous data in humans have utilized aggregate measures of single units and LFPs in the temporal lobe to show that neurophysiological states drift slowly over longer timescales (37, 40, 41). These drift measurements may provide coarse temporal information, and the relationship between these aggregate estimates of activity and the precise information provided by time cells (or information over the scales provided by ramping cells) remains a key area for further investigation.

Our findings connecting the consistency of time cell firing and temporal clustering behavior explicate a core feature of human memory, as the relationship we report fits with the hypothesized role of time cells in the representation of temporal information. This finding further establishes a possible link between time cells and place cells. Data in rodents and primates suggest that variability in place cell firing (analogous to our ρ measurement) reflects the representation of item and contextual features beyond spatial information (42, 43). Additionally, rodent place cells generally preferentially encode distance traveled, or less frequently, time elapsed, instead of spatial information while exploring virtual environments (44) and treadmill running (3). Further investigations can determine whether the spiking activity of subpopulations of time cells may additionally encode item-level information such as semantic category or reward conditions, depending upon the task. A complete understanding of time cells in humans will ultimately require identifying what additional information may be encoded by these cells and how they respond to different task demands (4, 23, 45). Related to this point, our observations suggest that human time cells are more broadly tuned than time cells observed in rodents (1, 2). Specific memory conditions that favor more precise temporal tuning such as shorter temporal contextual durations, or a memory probe that requires making temporal judgements, may identify more precisely tuned cells.

Our finding that time cells demonstrate theta precession during memory encoding links this phenomenon to human memory. Precession in the representation of temporal information provides neuron-level data to complement previous human LFP studies demonstrating the importance of gamma–theta oscillatory nesting to sequence learning (46, 47). It should be noted that our data suggest that phase precession may be less common in humans compared with rodents in terms of the fraction of time cells exhibiting precession (1). It is possible that the comparative complexity of our task to rodent paradigms, or the diversity of the frequencies that characterize human theta oscillations (32), attenuates our ability to observe phase precession. However, it may be the case that phase precession is not as ubiquitous in humans as in rodents for cells encoding contextual information, as instances of precession in human place cells have yet to be reported following years of investigation. Further work is needed to more exhaustively explore and characterize this important

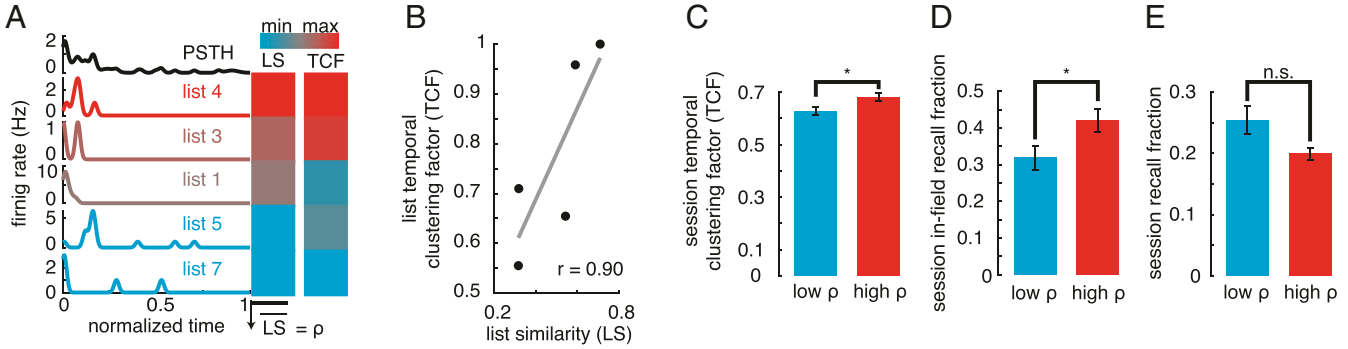

Fig. 7. Time cell stability promotes temporal clustering and influences which serial positions are recalled. (*A* and *B*) Illustration of calculating ρ and TCF. (*A*) Single-cell example of the correlation between time cell firing pattern similarity (list similarity [LS]) and temporal clustering (TCF). (*B*) Scatterplot demonstrating a positive list-level association between LS and TCF for the example neuron from *A*. ρ equals the average LS. (*C*) Comparison of mean session-wide temporal clustering between cells with high and low ρ. Bars represent mean values, and error bars represent the SEM. (*D*) Comparison of mean session-wide in-field performance between cells with high and low ρ. Bars represent mean values, and error bars represent the SEM. (*E*) Comparison of mean session-wide performance between cells with high and low ρ. Bars represent mean values, and error bars represent the SEM. n.s., not significant. *$P < 0.05$.

phenomenon, especially the specific instances that may or may not elicit significant precession in cells encoding spatial or temporal contextual information. Rodent data provide some guidance on this point as precession is less pronounced during passive compared with active locomotion (10). Our data may echo this finding, as the immediate context experienced by participants during memory retrieval is not mnemonically relevant. Rather, they are retrieving items from a previous contextual environment. Thus, precession may be generally more prevalent when the context over which spike-phase precesses, whether position or time, assumes behavioral salience.

Unique Roles of Ramping and Time Cells. As previously observed in rodents (11), we identified a population of neurons, prevalent in the entorhinal cortex, of cells that demonstrate ramping activity across temporal epochs of various lengths. In our data and in rodents, ramping cells reliably map out the temporal dimensions of a given task, without extensive or explicit training (Fig. 5*B*) (11), a crucial feature in real-world episodic memory formation. As time cell activity also depends on both temporal and extratemporal contextual features (Fig. 4 *E* and *F*) (1, 2, 23), ramping cells may serve as the link between temporal context and the selection of the hippocampal time cell population for a given task (12, 14, 48). In fact, several neurocomputational models explicitly generate time cells with the input activity of exponentially decaying cells (12–14). In this regard, ramping cells specifically may connect representations at different timescales by modulating hippocampal time cell activity. Like past ramping cell studies, we could not control for all potential covariates of time that naturally rise or decay throughout an experiment or behavioral epoch, such as neural fatigue (49) or the expectation of the end of a list. However, rather than explicitly tracking metric time, ramping cells may represent time inherently (18), integrating time out of evolving experience (11). If this is the case, phenomena such as fatigue or expectation may facilitate the generation of this inherent understanding of time, rather than provide an alternative explanation for ramping cell behavior.

We used distinct methods to identify time cells and ramping cells, limiting our ability to make direct comparisons or test for overlap in these populations. However, studies in animals support a nuanced distinction between time cells and ramping cells. For example, previous work has demonstrated that hippocampal CA1 time cells can represent time across seconds, minutes, and even days (24), similar to suggested characteristics of ramping cells (11). Previous rodent studies have demonstrated ramping cells in the hippocampus and subiculum (27, 28), blurring the sharp anatomical partitioning proposed by other recent work (11, 14). Furthermore, multiple studies have demonstrated the presence of time cells in the MEC (5, 22) or even extratemporal regions (23), demonstrating that rate coding of elapsed time on the order of seconds is not a uniquely hippocampal phenomenon. Future work with a common time and ramping cell modeling framework and increased precision of electrode localization within the entorhinal cortex is needed to fully elucidate the regional specificity of these cell types in humans.

Time Cells and Human Disease. The identification of time cells in the human temporal lobe and their connection with temporal clustering behavior carry potential implications for neuromodulation strategies to treat human disease. Namely, experimental interventions that enhance the fidelity of the temporal signal provided by time cells (as measured by ρ for example) could reduce the associative deficit characteristic of degenerative conditions as well as normal aging (50). Observing the impact of temporal and extratemporal stimulation strategies on time cell activity (51, 52) represents an opportunity to link these findings.

Conclusion

The temporal organization of memories constitutes a key function of the medial temporal lobe (53). The discovery of time cells that we report establishes a direct neurophysiological mechanism for the representation of temporal contextual information that is necessary for this function. The connection between time cell activity and temporal clustering behavior corroborates models of episodic memory that emphasize temporal coding and lays the foundations for future directions in the study of human memory.

Materials and Methods

Subjects and Electrophysiology. We consented a total of 27 human epilepsy patients undergoing clinical seizure mapping at either Thomas Jefferson University Hospital (TJUH) or University of Texas Southwestern Medical Center (UTSW) for enrollment in the study. The institutional review boards of both institutions approved this study. Each participant provided informed consent. The 27 subjects completed a total of 40 sessions of the memory task. We treated each session as independent for purposes of statistical analyses. Patients were implanted with depth electrodes at locations dictated by clinical interest. Electrodes featured both macroelectrode contacts along their length and 9 × 40-μm platinum–iridium microwires extruding from the tip. We sampled the broadband signal at either 30 kHz with NeuroPort (Blackrock Microsystems, UTSW) or 32.6 kHz with Cheetah (Neuralynx, TJUH) recording systems. We localized the microwires by coregistering post-implantation computed tomography scans with preoperative MRI. Neuroradiologists then confirmed localizations by anatomical landmarks. Boundaries of the entorhinal cortex, and within the MTL more generally, followed well-established methods (54–56). We excluded neurons from any channel not localized to a specific MTL subregion from further analysis (n = 34). Manual review showed that these often localized to white matter, the cistern, temporal horn, etc. We used BrainNet Viewer (57) to visualize electrode localizations.

We rejected sessions with clinically evident seizure activity or aura (one session, as determined by clinical report of attending epileptologists at the time of data collection). The clinical team additionally flagged channels exhibiting excessive noise or frequent interictal activity, which were excluded following previous methods (56). We excluded all microelectrode channels adjacent to the macroelectrode contact exhibiting this activity from analysis. All channels exhibiting seizure activity at any point were also flagged, although not excluded (and incorporated into our control analysis). Before spike detection and sorting, we band-pass filtered the broadband signal from 300 to 1,000 Hz and cleaned it with a volume conduction subtraction algorithm (58). This algorithm abates the influence of frequency-dependent noise present across electrodes. We made no specific effort to detect and reject high-frequency oscillation (HFO) events (59), although this algorithm reduces the impact of large-amplitude deflections occurring across the microelectrode channels on the signal passed on to the spike detection routine. We acknowledge that the influence of pathological vs. physiological HFOs on ripple events remains an active area of further investigation. Finally, we reidentified time cells using only channels free of seizure and interictal activity throughout the clinical recording period (control analysis results are displayed in *SI Appendix*, Tables S3 and S4).

Following denoising, we then used Combinato (60) for spike detection and clustering. Putative units were manually reviewed by author G.U. for 1) shape of the mean spike waveform, 2) number of interspike intervals (ISIs) below a threshold of 3 ms, 3) shape of the ISI distribution, 4) stationarity of unit spiking, and 5) similarity to other mean spike waveforms isolated from the same microwire. Based on these criteria, we either merged or discarded putative units prior to any subsequent analysis. For all microwires with more than one isolated unit, we calculated pairwise isolation distances (61) to examine the degree of separation of unit from units. We isolated a total of 768 units (also referred to as "cells" and "neurons" throughout the manuscript). Only putative pyramidal cells located in either the entorhinal cortex or hippocampus (509/768) were considered for all time cell analyses. We identified these as units with a firing rate of less than 5 Hz (8, 62, 63) and with a "wide" (>0.40-ms) spike width (64). We defined the spike width as the trough-to-peak time (21). Hartigan's Dip test confirmed bimodality of the spike width distribution ($P < 0.001$) (21). We then fit a fourth-order polynomial to the data and used the spike width at the local minimum that split the two modes of the distribution (0.40 ms) to divide units into those with "narrow" and wide spike widths.

For all 768 units isolated, we computed quality metrics as reported in a similar, large, human, single-unit dataset (21). Units isolated per channel, mean firing rate, percentage of ISI less than 3 ms, modified coefficient of

variation, signal-to-noise ratio of both the peak of the mean waveform and the mean of the mean waveform, and isolation distance distributions were all comparable with this reference high-quality dataset. These data are displayed in *SI Appendix*, Fig. S2 and Table S1.

When the phase of the theta LFP was required for an analysis, we first low-pass filtered the signal at 300 Hz. We then applied a notch filter at 60 Hz. Finally, we down sampled the signal by a factor of 30 or 32, depending on the original sampling rate. Phase was then extracted by convolving six evenly log-spaced Morlet wavelets, all with a width of six, at frequencies between 1.68 and 9.51 Hz.

Behavioral Task. Subjects completed a free recall task, delivered at clinical bedside via a laptop computer. The task consisted of a repeating encoding–distractor–retrieval paradigm. During the encoding section, patients studied a sequence of words that appeared on the screen. All presented words were monosyllabic nouns. Words only appeared once per session. We used the Corpus of Contemporary American English (https://www.wordfrequency.info/) (65) to estimate word frequency. Word frequency values range from 485 to 331,597 occurrences per 1 billion words. The most common word included, "world," ranks 123rd among all English words, while the least common word, "slush," ranks 19,291st. Each word stayed on screen for 1.6 s. A 0.8- to 1.2-s jitter period separated neighboring words. TJUH subjects studied 15-word lists. UTSW subjects studied 12-word lists. During the distractor period, participants completed simple arithmetic problems for at least 20 s. All problems followed the format of A + B + C = ?. Following this, subjects entered into a 30-s (UTSW) or 45-s (TJUH) retrieval phase, during which they recalled as many words as able from the most recently studied word list. Subjects were allowed breaks in between word lists. Subjects repeated this sequence for as many lists as they could, ranging from 4 to 25, depending on the subject and session. For all analyses save the performance vs. serial position behavioral analysis, sessions with 15-word lists and 12-word lists were considered together.

We told participants how many words they would see on each list and how long they would have to recall words following each list. We did not explicitly communicate the duration of encoding lists to the participants; however, it is reasonable to assume they developed an expectation from the information shared and from experience on the practice lists completed before formal testing began.

Time Cell Identification. We utilized a nonparametric binning procedure to identify time cells without assuming anything about the nature of the relationship between cell firing rate and time. This method is similar to previous work identifying human place cells (56). First, we convolved the session-wide spike train with a Gaussian kernel with an SD of 0.5 s in order to obtain an instantaneous firing rate at every sample in the recording. We refer to the convoluted spike train as the session-wide "tuning curve" throughout the manuscript. For encoding time cells, we then pulled the sections of this tuning curve corresponding to each of the encoding lists. Encoding lists lasted from 30 to 40 s. For retrieval time cells, we used sections of the tuning curve corresponding to each of the retrieval lists. Retrieval lists lasted from 30 to 45 s. These tuning curves were then aligned by normalizing the time domain to account for small differences in absolute time from list to list due to interword jitter. We did this by first generating a one-by-list sample vector with values ranging from one to the total number of samples on that list. We then divided each value by the total number of samples on that list. Next, we evenly distributed all these samples into 40 time bins based on this normalized sample vector. For each time bin, we calculated the mean of the tuning curve firing rate at all samples falling within that bin. Time bins ranged in absolute time from roughly 0.75 to 1.1 s, depending on jitter and number of words on the list. After constructing a list-by-time bin matrix, we tested for temporal modulation of firing rate with a Kruskal–Wallis test. We chose a mean rank-based test to limit the influence of a single instance of a high firing rate in a given time bin and because firing rate is Poisson, not normally, distributed. We passed cells with a $p_{actual} < 0.05$ with this procedure to the next step of testing. We subjected all passing cells to permutation testing to confirm above chance temporal modulation of firing rate. To do this, we randomly circularly shuffled the session-wide tuning curve and then repeated the described procedure. We did this 1,000 times for each cell. $p_{shuffle}$ was obtained by comparing p_{actual} with the distribution of P values obtained from the permutation procedure. We defined $p_{shuffle}$ as the number of shuffles producing a smaller P value than p_{actual}, divided by 1,000. Only potential time cells with $p_{shuffle} < 0.05$ were ultimately considered time cells. This model did not assume a specific relationship between time and firing rate, only that time modulates firing rate. This means that time cells were not required to have a single temporal field of increased activity. We note that the time cell population heat maps are not central to the identification of time cells but are rather used to display population-level data in a manner consistent with previous time cell studies (1, 2, 6, 24). While we extensively controlled these results with alternative time cell identification methodologies, all central results and figures communicate the results of our principal Kruskal–Wallis, shuffled-based method described in this section. We prefer this method as it properly models firing rate nonparametrically and makes fewer assumptions than other frameworks, such as maximum likelihood estimation-based models.

Precession. We calculated precession on the all-list, all-spikes level within the peak time field of each time cell. We used circular–linear correlation methods, as previously described (29, 66), as they are less prone to inconsistencies due to low spike counts or noise (29, 30). We did this by fitting the following nonlinear model, relating theta phase to time:

$$\psi = 2\pi s t + \psi_0,$$

where "ψ" is the circular variable theta phase, "s" is the slope describing the relationship, "t" is the linear variable time, and "ψ_0" is the phase offset. We fit this model by maximizing the length of the mean resultant, given by the following equation, with matlab's fminbnd:

$$R(s) = \sqrt{\left[\frac{1}{n}\sum_{j=1}^{n}\cos\left(\psi_j - 2\pi s t_j\right)\right]^2 + \left[\frac{1}{n}\sum_{j=1}^{n}\sin\left(\psi_j - 2\pi s t_j\right)\right]^2},$$

where "n" represents the number of in-field spikes. The solver was bound such that the slope could only range from 0 to $\pm 4\pi$ (30). A time field was said to be precessing if the slope relating phase to time was less than zero. However, a field was said to demonstrate significant precession on the basis of the circular–circular correlation coefficient obtained after transforming time into a circular variable (29, 67). Due to the heterogeneity of human theta, we repeated the above procedure at each of six log-spaced frequencies within the theta band for each time cell.

We false discovery rate (FDR) corrected the resulting vector of P values obtained for each cell across frequencies with a Q of 0.20. We then tested the fraction of surviving cells against chance with a one-sided binomial test with an FDR of Q. We tested phase distributions against the null hypothesis of uniformity with a Rayleigh test. We computed all circular statistics with the matlab toolbox developed by Berens (67).

We used a shuffle control to confirm that the proportion of time cells demonstrating precessing during encoding and retrieval was above chance. For this, we randomly shuffled the spike phases and then, separately, the spike times 1,000 times, repeating our statistical methods as described above. We compared our actual yield of precessing cells with the distribution of precessing cells from each shuffle. We defined our P value as the number of shuffles leading to identification of more precessing cells than in our actual data divided by the number of shuffles.

We assessed the theta power present during time cell precession. For each cell demonstrating precession, we extracted LFP data from the microwire channel from which we isolated that cell. We then extracted the power at the theta frequency over which that cell demonstrated precession. After log transforming the power values (with the natural logarithm), we took the average theta power within the time field of that cell (i.e., when the cell demonstrated precession). We additionally calculated the average power value across all time points across encoding (for encoding time cells) or retrieval (for retrieval time cells) periods outside of that cell's time field. We then computed the pairwise difference between these two values and tested for a significant increase in power with a one-sample t test against zero.

For display purposes only, we generated a precession heat map by plotting all spikes from the central 25% of all time cells demonstrating precession on the same set of axes (Fig. 6*C*). For this, we binned all spikes into 100 equally sized bins, with 10 time partitions and 10 phase partitions. The domain of each bin covered 2.5% of the time cell's time field, and the range of each bin covered 72°.

We included two population-level metrics of precession. First, for encoding and retrieval time cells separately, we summed all correlation coefficients across cells. Then, we randomly shuffled each cell's spike time–phase pairs 1,000 times, recomputing the sum across cells each time. We then compared the real sum with the shuffle distribution to obtain a P value for both encoding (*SI Appendix*, Fig. S7*C*) and retrieval (*SI Appendix*, Fig. S7*D*) time cell populations.

Second, we adopted the three main analyses of Harris et al. (35). First, we correlated the instantaneous firing rate of each time cell for each of its spikes with the theta phase associated with each spike. We calculated the

instantaneous firing rate by counting the number of spikes in a window from 360° before and to 360° after the observed spike phase. We obtained the spike phase with a Hilbert transform and a theta band of 2 to 10 Hz. We then took the circular mean phase across all spikes for each firing rate group (Fig. 6*D* and *SI Appendix*, Fig. S7*E*). We assessed for an association between firing rate and mean phase with a nonparametric circular ANOVA (35). We only included firing rate groups with at least 10 spikes (67). We assessed for a directional correlation with a one-sided Spearman rank correlation.

Next, we compared the circular mean spike phase during periods of firing rate acceleration "onset" with that during periods of firing rate deceleration "offset." For a spike to qualify for inclusion in the onset group, the previous eight theta cycles could have no more than two total spikes (~1.4 Hz), and the subsequent eight theta cycles must have at least eight spikes (~5.5 Hz). For a spike to qualify for the offset group, the previous eight theta cycles must have at least eight spikes, and the subsequent eight theta cycles could have no more than two spikes. We then compared the circular median spike phases between groups (Fig. 6*E* and *SI Appendix*, Fig. S7*F*).

Finally, we correlated the spike rate derivative, or spike acceleration, with spike phase. We calculated the spike rate derivate by counting the number of spikes within the theta cycle of the index spike and within the three theta cycles preceding and following the index spike. We fit a linear model to the spike count vs. theta cycle distribution and used the slope as the spike rate derivative. We then looked for a directional correlation between rate derivative and spike phase (Fig. 6*F* and *SI Appendix*, Fig. S7*G*).

Behavioral Analyses. We used the mean list-to-mean tuning curve correlation, ρ, as the predictor variable in the behavioral analyses. We calculated this by correlating all of the individual list tuning curves with the cross-list mean tuning curve (PSTH) and averaging the resulting Spearman rank correlation coefficients. This metric is not a statistical validation of the robustness of the temporal specificity of our time cells, which rather is demonstrated with our main time cell identification method and numerous controls (*SI Appendix*, Tables S3 and S4), but instead, is a measure of the consistency in the temporal modulation of firing rate across the recording session. We refer to this idea as "consistency" or "stability" in the time field representation. When we used two-group testing with this predictor, we split values at the median.

We used temporal clustering at retrieval as the main behavioral outcome variables. Temporal clustering was calculated as previously published (68). In brief, for each retrieval period, all transitions between recalled words were considered. If there were four words recalled on a list, then there were three transitions between them. For example, "queen" to "world" counted as a transition. The difference in encoding serial positions for both words of the transition was then obtained. Each transition received a score based on where the actual transition serial position difference ranked among all possible remaining transitions. Because of the noise of this metric on a single-list level, we computed the metric across the entire session by averaging all transitions made throughout the session. Due to the nature of the metric, only encoding lists from which subjects recalled at least two words contributed.

While both ρ and temporal clustering are defined on a subject (session) level to reduce noise, in Fig. 7 *A* and *B* we illustrate the relationship between time cell stability and temporal clustering on the list level. In Fig. 7*B*, the *x* value represents the Spearman correlation between that list's temporal tuning curve and the average temporal tuning curve across all lists (referred to as the PSTH in the manuscript). The cross-list average of all these correlations is ρ. The *y* value represents the single-list TCF.

We used a two-sample Kolmogorov–Smirnov test to assess the similarity between the performance-by-serial position curve and the peak count-by-serial position curve. We obtained the latter by counting the number of encoding time cell PSTHs that peaked within each of the serial positions. We then normalized both curves to their respective minimum and maximum values to obtain unitless, comparable curves. To control for differences in the performance vs. serial position curve between recording sessions in which subjects were presented with 12-word lists and 15-word lists, we considered these sessions separately.

We identified a session-level temporal contiguity effect (Fig. 1*G*) by calculating the recall probability for each encoding serial position based on the temporal proximity at encoding to the word just recalled. We assessed for an association between the primacy effect and time cells with early firing fields by defining "primacy time cells" as those with time fields covering the first encoding serial position (*SI Appendix*, Fig. S8). We defined significant primacy effects on the session level with a binomial test. We considered the number of successes the number of encoding lists from which participants correctly recalled the first serial position and the chance rate equal to the overall performance across the session.

Data Availability. Code data have been deposited in Mendeley Data (http://dx.doi.org/10.17632/2pzjthx2k3.1).

ACKNOWLEDGMENTS. We thank G. Konopka and Z. Tiganj for helpful remarks on the manuscript. We are grateful for all the patients who volunteered to participate in this study. This work was funded by NIH Research Project Grants R01-MH104606 (to J.J.), R01-MH55687 (to M.K.), and R01-NS107357 (to B.L.), as well as by support from the Southwestern Medical Foundation (B.E.P.) and the THR clinical scholars program (B.L.).

1. E. Pastalkova, V. Itskov, A. Amarasingham, G. Buzsáki, Internally generated cell assembly sequences in the rat hippocampus. *Science* **321**, 1322–1327 (2008).
2. C. J. MacDonald, K. Q. Lepage, U. T. Eden, H. Eichenbaum, Hippocampal "time cells" bridge the gap in memory for discontiguous events. *Neuron* **71**, 737–749 (2011).
3. B. J. Kraus, R. J. Robinson II, J. A. White, H. Eichenbaum, M. E. Hasselmo, Hippocampal "time cells": Time versus path integration. *Neuron* **78**, 1090–1101 (2013).
4. C. J. MacDonald, S. Carrow, R. Place, H. Eichenbaum, Distinct hippocampal time cell sequences represent odor memories in immobilized rats. *J. Neurosci.* **33**, 14607–14616 (2013).
5. B. J. Kraus *et al*., During running in place, grid cells integrate elapsed time and distance run. *Neuron* **88**, 578–589 (2015).
6. D. M. Salz *et al*., Time cells in hippocampal area CA3. *J. Neurosci.* **36**, 7476–7484 (2016).
7. J. R. Manns, M. W. Howard, H. Eichenbaum, Gradual changes in hippocampal activity support remembering the order of events. *Neuron* **56**, 530–540 (2007).
8. W. E. Skaggs, B. L. McNaughton, M. A. Wilson, C. A. Barnes, Theta phase precession in hippocampal neuronal populations and the compression of temporal sequences. *Hippocampus* **6**, 149–172 (1996).
9. J. C. Magee, D. Johnston, A synaptically controlled, associative signal for Hebbian plasticity in hippocampal neurons. *Science* **275**, 209–213 (1997).
10. C. Drieu, R. Todorova, M. Zugaro, Nested sequences of hippocampal assemblies during behavior support subsequent sleep replay. *Science* **362**, 675–679 (2018).
11. A. Tsao *et al*., Integrating time from experience in the lateral entorhinal cortex. *Nature* **561**, 57–62 (2018).
12. M. W. Howard *et al*., A unified mathematical framework for coding time, space, and sequences in the hippocampal region. *J. Neurosci.* **34**, 4692–4707 (2014).
13. Y. Liu, Z. Tiganj, M. E. Hasselmo, M. W. Howard, A neural microcircuit model for a scalable scale-invariant representation of time. *Hippocampus* **29**, 260–274 (2019).
14. E. T. Rolls, P. Mills, The generation of time in the hippocampal memory system. *Cell Rep.* **28**, 1649–1658.e6 (2019).
15. M. Fyhn, S. Molden, M. P. Witter, E. I. Moser, M. B. Moser, Spatial representation in the entorhinal cortex. *Science* **305**, 1258–1264 (2004).
16. N. J. Killian, M. J. Jutras, E. A. Buffalo, A map of visual space in the primate entorhinal cortex. *Nature* **491**, 761–764 (2012).
17. J. Jacobs *et al*., Direct recordings of grid-like neuronal activity in human spatial navigation. *Nat. Neurosci.* **16**, 1188–1190 (2013).
18. G. Buzsáki, R. Llinás, Space and time in the brain. *Science* **358**, 482–485 (2017).
19. M. E. Hasselmo, A model of episodic memory: Mental time travel along encoded trajectories using grid cells. *Neurobiol. Learn. Mem.* **92**, 559–573 (2009).
20. P. B. Sederberg *et al*., Oscillatory correlates of the primacy effect in episodic memory. *Neuroimage* **32**, 1422–1431 (2006).
21. M. C. M. Faraut *et al*., Dataset of human medial temporal lobe single neuron activity during declarative memory encoding and recognition. *Sci. Data* **5**, 180010 (2018).
22. J. G. Heys, D. A. Dombeck, Evidence for a subcircuit in medial entorhinal cortex representing elapsed time during immobility. *Nat. Neurosci.* **21**, 1574–1582 (2018).
23. Z. Tiganj, J. A. Cromer, J. E. Roy, E. K. Miller, M. W. Howard, Compressed timeline of recent experience in monkey lateral prefrontal cortex. *J. Cogn. Neurosci.* **30**, 935–950 (2018).
24. W. Mau *et al*., The same hippocampal CA1 population simultaneously codes temporal information over multiple timescales. *Curr. Biol.* **28**, 1499–1508.e4 (2018).
25. K. B. Kjelstrup *et al*., Finite scale of spatial representation in the hippocampus. *Science* **321**, 140–143 (2008).
26. B. A. Strange, M. P. Witter, E. S. Lein, E. I. Moser, Functional organization of the hippocampal longitudinal axis. *Nat. Rev. Neurosci.* **15**, 655–669 (2014).
27. B. Young, N. McNaughton, Common firing patterns of hippocampal cells in a differential reinforcement of low rates of response schedule. *J. Neurosci.* **20**, 7043–7051 (2000).
28. R. E. Hampson, S. A. Deadwyler, Temporal firing characteristics and the strategic role of subicular neurons in short-term memory. *Hippocampus* **13**, 529–541 (2003).
29. R. Kempter, C. Leibold, G. Buzsáki, K. Diba, R. Schmidt, Quantifying circular-linear associations: Hippocampal phase precession. *J. Neurosci. Methods* **207**, 113–124 (2012).
30. R. Schmidt *et al*., Single-trial phase precession in the hippocampus. *J. Neurosci.* **29**, 13232–13241 (2009).
31. U. Rutishauser, I. B. Ross, A. N. Mamelak, E. M. Schuman, Human memory strength is predicted by theta-frequency phase-locking of single neurons. *Nature* **464**, 903–907 (2010).

32. J. Jacobs, Hippocampal theta oscillations are slower in humans than in rodents: Implications for models of spatial navigation and memory. *Philos. Trans. R. Soc. Lond. B Biol. Sci.* **369**, 20130304 (2013).
33. J. Miller *et al*., Lateralized hippocampal oscillations underlie distinct aspects of human spatial memory and navigation. *Nat. Commun.* **9**, 2423 (2018).
34. J. O'Keefe, M. L. Recce, Phase relationship between hippocampal place units and the EEG theta rhythm. *Hippocampus* **3**, 317–330 (1993).
35. K. D. Harris *et al*., Spike train dynamics predicts theta-related phase precession in hippocampal pyramidal cells. *Nature* **417**, 738–741 (2002).
36. M. W. Howard, M. J. Kahana, A distributed representation of temporal context. *J. Math. Psychol.* **46**, 269–299 (2002).
37. J. R. Manning, S. M. Polyn, G. H. Baltuch, B. Litt, M. J. Kahana, Oscillatory patterns in temporal lobe reveal context reinstatement during memory search. *Proc. Natl. Acad. Sci. U.S.A.* **108**, 12893–12897 (2011).
38. E. Tulving, Episodic memory: From mind to brain. *Annu. Rev. Psychol.* **53**, 1–25 (2002).
39. S. M. Polyn, K. A. Norman, M. J. Kahana, A context maintenance and retrieval model of organizational processes in free recall. *Psychol. Rev.* **116**, 129–156 (2009).
40. M. W. Howard, I. V. Viskontas, K. H. Shankar, I. Fried, Ensembles of human MTL neurons "jump back in time" in response to a repeated stimulus. *Hippocampus* **22**, 1833–1847 (2012).
41. S. Folkerts, U. Rutishauser, M. W. Howard, Human episodic memory retrieval is accompanied by a neural contiguity effect. *J. Neurosci.* **38**, 4200–4211 (2018).
42. A. A. Fenton, R. U. Muller, Place cell discharge is extremely variable during individual passes of the rat through the firing field. *Proc. Natl. Acad. Sci. U.S.A.* **95**, 3182–3187 (1998).
43. R. A. Gulli *et al*., Context-dependent representations of objects and space in the primate hippocampus during virtual navigation. *Nat. Neurosci.* **23**, 103–112 (2020).
44. P. Ravassard *et al*., Multisensory control of hippocampal spatiotemporal selectivity. *Science* **340**, 1342–1346 (2013).
45. S. Terada, Y. Sakurai, H. Nakahara, S. Fujisawa, Temporal and rate coding for discrete event sequences in the hippocampus. *Neuron* **94**, 1248–1262.e4 (2017).
46. A. C. Heusser, D. Poeppel, Y. Ezzyat, L. Davachi, Episodic sequence memory is supported by a theta-gamma phase code. *Nat. Neurosci.* **19**, 1374–1380 (2016).
47. A. Bahramisharif, O. Jensen, J. Jacobs, J. Lisman, Serial representation of items during working memory maintenance at letter-selective cortical sites. *PLoS Biol.* **16**, e2003805 (2018).
48. J. L. Bellmund, P. Gärdenfors, E. I. Moser, C.F. Doeller, Navigating cognition: Spatial codes for human thinking. *Science* **362**, eaat6766 (2018).
49. M. D. Serruya, P. B. Sederberg, M. J. Kahana, Power shifts track serial position and modulate encoding in human episodic memory. *Cereb. Cortex* **24**, 403–413 (2014).
50. M. Naveh-Benjamin, Z. Hussain, J. Guez, M. Bar-On, Adult age differences in episodic memory: Further support for an associative-deficit hypothesis. *J. Exp. Psychol. Learn. Mem. Cogn.* **29**, 826–837 (2003).
51. Y. Ezzyat *et al*., Closed-loop stimulation of temporal cortex rescues functional networks and improves memory. *Nat. Commun.* **9**, 365 (2018).
52. V. S. Natu *et al*., Stimulation of the posterior cingulate cortex impairs episodic memory encoding. *J. Neurosci.* **39**, 7173–7182 (2019).
53. N. M. Long, M. J. Kahana, Hippocampal contributions to serial-order memory. *Hippocampus* **29**, 252–259 (2019).
54. A. Ekstrom *et al*., High-resolution depth electrode localization and imaging in patients with pharmacologically intractable epilepsy. *J. Neurosurg.* **108**, 812–815 (2008).
55. N. Suthana *et al*., Memory enhancement and deep-brain stimulation of the entorhinal area. *N. Engl. J. Med.* **366**, 502–510 (2012).
56. S. E. Qasim *et al*., Memory retrieval modulates spatial tuning of single neurons in the human entorhinal cortex. *Nat. Neurosci.* **22**, 2078–2086 (2019).
57. M. Xia, J. Wang, Y. He, BrainNet viewer: A network visualization tool for human brain connectomics. *PLoS One* **8**, e68910 (2013).
58. S. Kota *et al*., "A frequency based spatial filter to mitigate volume conduction in electroencephalogram signals" in *2016 38th Annual International Conference of the IEEE Engineering in Medicine and Biology Society, J. Patton, Ed.*, (IEEE, Orlando, FL, 2016), pp. 4001–4004.
59. S. Liu, J. Parvizi, Cognitive refractory state caused by spontaneous epileptic high-frequency oscillations in the human brain. *Sci. Transl. Med.* **11**, eaax7830 (2019).
60. J. Niediek, J. Boström, C. E. Elger, F. Mormann, Reliable analysis of single-unit recordings from the human brain under noisy conditions: Tracking neurons over hours. *PLoS One* **11**, e0166598 (2016).
61. N. Schmitzer-Torbert, J. Jackson, D. Henze, K. Harris, A. D. Redish, Quantitative measures of cluster quality for use in extracellular recordings. *Neuroscience* **131**, 1–11 (2005).
62. T. J. Davidson, F. Kloosterman, M. A. Wilson, Hippocampal replay of extended experience. *Neuron* **63**, 497–507 (2009).
63. M. J. Ison *et al*., Selectivity of pyramidal cells and interneurons in the human medial temporal lobe. *J. Neurophysiol.* **106**, 1713–1721 (2011).
64. D. J. Foster, M. A. Wilson, Hippocampal theta sequences. *Hippocampus* **17**, 1093–1099 (2007).
65. M. Davies, The 385+ million word corpus of contemporary American English (1990–2008+): Design, architecture, and linguistic insights. *Int. J. Corpus Linguist.* **14**, 159–190 (2009).
66. E. T. Reifenstein, R. Kempter, S. Schreiber, M. B. Stemmler, A. V. Herz, Grid cells in rat entorhinal cortex encode physical space with independent firing fields and phase precession at the single-trial level. *Proc. Natl. Acad. Sci. U.S.A.* **109**, 6301–6306 (2012).
67. P. Berens, CircStat: A MATLAB toolbox for circular statistics. *J. Stat. Softw.* **31**, 39160 (2009).
68. P. B. Sederberg, J. F. Miller, M. W. Howard, M. J. Kahana, The temporal contiguity effect predicts episodic memory performance. *Mem. Cognit.* **38**, 689–699 (2010).